Optical properties of ZnO and ZnO:In nanorods assembled by sol-gel method

Y. W. Chen, Y. C. Liu, S. X. Lu, C. S. Xu, C. L. Shao et al.

Citation: J. Chem. Phys. **123**, 134701 (2005); doi: 10.1063/1.2009731
View online: http://dx.doi.org/10.1063/1.2009731
View Table of Contents: http://jcp.aip.org/resource/1/JCPSA6/v123/i13
Published by the American Institute of Physics.

Optical properties of ZnO and ZnO:In nanorods assembled by sol-gel method

Y. W. Chen
Center for Advanced Optoelectronic Functional Material Research, Northeast Normal University, Changchun 130024, People's Republic of China and Key Laboratory of Excited State Processes, Changchun Institute of Optics, Fine Mechanics and Physics, Chinese Academy of Sciences, Changchun 130033, People's Republic of China

Y. C. Liu[a)]
Center for Advanced Optoelectronic Functional Material Research, Northeast Normal University, Changchun 130024, People's Republic of China

S. X. Lu
Department of Chemistry, School of Science, Beijing Institute of Technology, Beijing 100081, People's Republic of China

C. S. Xu and C. L. Shao
Center for Advanced Optoelectronic Functional Material Research, Northeast Normal University, Changchun 130024, People's Republic of China

C. Wang, J. Y. Zhang, Y. M. Lu, D. Z. Shen, and X. W. Fan
Key Laboratory of Excited State Processes, Changchun Institute of Optics, Fine Mechanics and Physics, Chinese Academy of Sciences, Changchun 130033, People's Republic of China

(Received 31 May 2005; accepted 6 July 2005; published online 4 October 2005)

Self-assembled zinc oxide (ZnO) and indium-doping zinc oxide (ZnO:In) nanorod thin films were synthesized on quartz substrates without catalyst in aqueous solution by sol-gel method. The samples were characterized by x-ray diffraction (XRD), scanning electron microscope (SEM), Raman-scattering spectroscopy, room-temperature photoluminescence (PL) spectra, and temperature-dependent PL spectra measurements. XRD and Raman spectra illustrated that there were no single In_2O_3 phase in ZnO lattice after indium doping. The PL spectra of ZnO showed a strong UV emission band located at 394 nm and a very weak visible emission associated with deep-level defects. Indium incorporation induced the shift of optical band gap, quenching of the near-band-edge photoluminescence and enhanced LO mode multiphonon resonant Raman scattering in ZnO crystals at different temperatures. Abnormal temperature dependence of UV emission integrated intensity of ZnO and ZnO:In samples is observed. The local state emission peak of ZnO:In samples at 3.37 eV is observed in low-temperature PL spectra. The near-band-edge emission peak at room temperature was a mixture of excitons and impurity-related transitions for both of two samples. © *2005 American Institute of Physics*. [DOI: 10.1063/1.2009731]

I. INTRODUCTION

ZnO, a direct wide-band-gap semiconductor (E_g =3.37 eV at room temperature) with a large exciton binding energy of 60 meV, is an ideal material for optoelectronic applications. The study of one-dimensional ZnO nanostructures, such as nanowires, nanobelts, and nanostructural arrays, has attracted extensive interests due to their excellent optical, electrical, gas-sensing, and piezoelectric properties.[1–5] Doping with selective elements offers an effective method to adjust the electrical, optical, and magnetic properties of ZnO, which is crucial for its practical application. Although a mass of research has been done on nanostructure doping, doped one-dimensional ZnO nanostructures have rarely been reported. It still remains a challenge to achieve high-quality crystalline with unique optical and electrical properties in doped one-dimensional ZnO nanostructures. Indium is recognized as one of the most efficient elements used to improve the optoelectrical properties of ZnO. Because In-doped ZnO has excellent optical transmission, high electrical conductivity, unique chemical stability, thermal stability, etc.,[6–10] it can be used in solar cell, transparent conducting electronics, etc. However, its quality is still not good enough for the realization of high efficiency devices. Thus, the study of optical and electrical properties of In-doped ZnO is important from both fundamental and applied points of view. Recently, In-doped ZnO nanowires and nanobelts were synthesized by thermal evaporation and vapor phase transport method.[11–13] These samples tend to show strongly varying properties depended on the conditions of the employed method. The growth temperatures of most ZnO nanowires and nanobelts are above 800 °C, making those methods incompatible with low-cost flexible substrates. However, so far as we know, In-doped ZnO nanorods

[a)]Author to whom correspondence should be addressed; FAX: +86-431-5684009; electronic mail: ycliu@nenu.edu.cn

synthesized by wet chemical processing have not been reported yet, and their optical and electrical properties still need a further research. This wet chemical synthetic approach provides a promising option for low-temperature (in aqueous solution at temperatures below 100 °C), large-scale production of ZnO on various substrates. This method is easily reproducible and applicable to large industrial scale fabrication of products at low cost. In this paper, we reported the self-assembled ZnO and In-doped ZnO nanorods in aqueous solution without catalyst by sol-gel method. The purpose of the work is to investigate the effects of indium doping on the structural and optical properties of ZnO nanorods.

II. EXPERIMENT

All the chemicals are analytic grade reagents without further purification and from Beijing Chemical company. The undoped and In-doped ZnO thin films were grown on quartz substrates, respectively, by sol-gel method. Zinc nitrate hexahydrate ($Zn(NO_3)_2 \cdot 6H_2O$) and methenamine ($C_6H_{12}N_4$) reacted in the condition of equimolar for 0.02 M. Substrates were placed vertically in aqueous solution of $Zn(NO_3)_2 \cdot 6H_2O$ and $C_6H_{12}N_4$ in the glass bottles at 95 °C for 2 h. This reaction condition is similar to the reference.[14] Doping was performed by adding 0.2-mM indium chloride ($InCl_3 \cdot 4H_2O$) to produce ZnO:In nanorods thin films.

To characterize the film structure, the XRD was measured using a D/max-RA XRD spectrometer (Rigaku) with a Cu $K\alpha$ line of 1.5418 Å. The surface morphology was studied with a SEM (Hitachi-600). To investigate the local vibration modes, Raman-scattering spectra were obtained on HR-800 LabRam confocal Raman microscope with a backscattering configuration made by JY company in France, excited by the 488-nm line of an argon-ion laser at room temperature. The optical properties were obtained by the PL measurements using HR800 LabRam Infinity Spectrophotometer excited by a continuous He–Cd laser with a wavelength of 325 nm at a power of 50 mW. Temperature-dependent PL studies were carried out by using liquid-nitrogen refrigeration equipment in the temperature range from 79 K to room temperature.

III. RESULTS AND DISCUSSION

Figure 1 shows XRD patterns of ZnO (a) and ZnO:In (b) nanorods grown on quartz substrates. The multipeaks in the XRD spectra of ZnO and ZnO:In nanorods indicate the formation of typical hexagonal wurtzite structures. The growth orientation (100) near 32.017° is dominant, and it illustrates that c axes of most grains are parallel to the substrate surface. No diffraction peaks of In or other impurities phases are found in any of our samples. Low-concentration In doping cannot induce multiphase appearance. Moreover, heavy doping in a limited concentration will not result in the emergence of multiphase if the experiment conditions are well controlled.[12] After In doping, the major diffraction peaks shift slightly towards smaller diffraction angle compared to the ZnO crystals, suggesting an increase of lattice constant. It is suggested that the larger In^{3+} substitutes the smaller Zn^{2+} site partly and leads to an increase in the lattice constant.

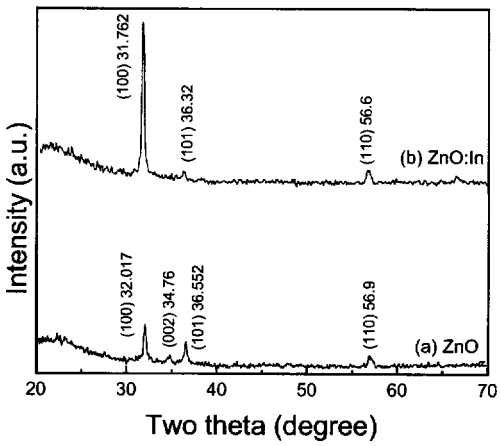

FIG. 1. XRD spectra of undoped and In-doped ZnO nanorods.

The morphology and microstructure of the as-grown materials were characterized and analyzed by SEM using a Hitach-600. SEM image (Fig. 2) shows that the as-grown products have a similar size and uniform rodlike shape with average diameter of about 250 nm and length up to about 3 μm. Well-aligned ZnO nanorods can be observed.

The room-temperature Raman spectra of ZnO and ZnO:In nanorods on quartz substrates excited by the 488 -nm line of Ar^+ laser are shown in Fig. 3. The wurtzite $C_{6v}^4(P6_3mc)$ symmetry of ZnO with two formula units in the primitive cell gives rise to optical-phonon modes classified as $A_1+E_1+2E_2+2B_1$.[15,16] Among these, the A_1+E_1 modes are both Raman and infrared active, and they are polar and split into transverse optical (TO) and longitudinal optical (LO) phonons. The two nonpolar E_2 modes (E_{2L} and E_{2H}) are only Raman active and the B_1 modes are infrared and Raman inactive (silent modes). According to the selection rules, both E_2 and A_1 modes are Raman active and expected in Raman spectra when the experiments are taken in a backscattering geometry. We observe E_{2H} modes at 437 cm^{-1} and $E_{2H}-E_{2L}$ modes at 334 cm^{-1} for both samples. One A_1 (TO) mode is located at 380 cm^{-1}. In addition, two LO phonon peaks can also be observed at 576 cm^{-1} (1LO) and 1147 cm^{-1} (2LO), as illustrated in Fig. 3. The frequency shift of 1LO phonon is 571 cm^{-1}. It illustrates that multiphonon resonant process in ZnO lattice can be observed. A_1 (TO) vibration mode at 380 cm^{-1} is not obvious, however, it makes the low-frequency side of E_{2H} mode widen.

The E_2 modes corresponds to characteristic band of wurtzite phase. The appearance of the LO phonon peak has

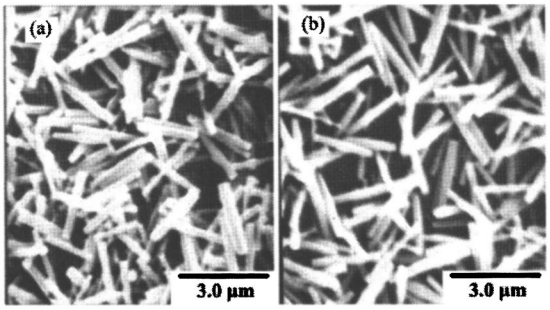

FIG. 2. SEM photos of the as-grown ZnO (a) and ZnO: In (b).

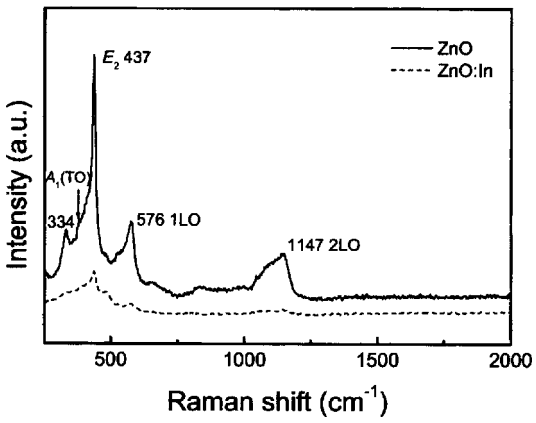

FIG. 3. Raman spectra of undoped and In-doped ZnO samples.

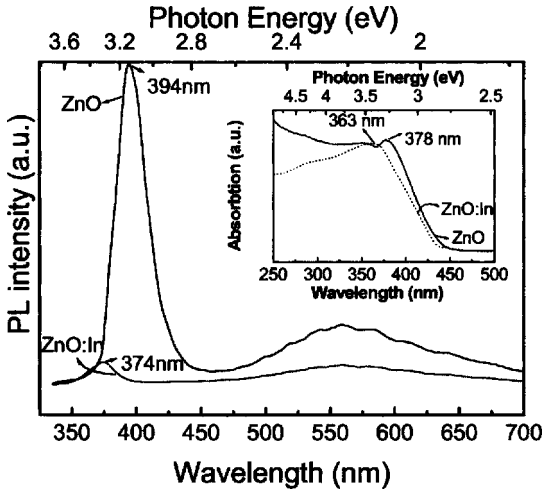

FIG. 4. PL spectrum of the ZnO and ZnO:In at room temperature.

been attributed to the formation of oxygen defects, interstitial Zn, and free carrier. Strong coupling of free carrier with LO phonon mode would cause broadening of linewidth, frequency down-shift, and asymmetric line shape. According to Fig. 3, the E_{2H} peak shows a dominant intensity over the LO phonon peak and a very sharp feature. It indicates that the wurtzite structure formed, ZnO and ZnO:In crystal quality is good, which is in agreement with XRD result. The broad feature of LO phonon peaks, especially 2LO phonon modes, can be ascribed to the defect electronic states within the band gap existing in both samples.

In contrast to Raman spectra of ZnO, the Raman-scattering peak position of ZnO:In does not change after In doping. Moreover, there are no Raman-scattering modes of In_2O_3. It can be concluded that there are no single In_2O_3 phase in ZnO lattice, which is consistent with XRD spectra. In addition, the intensity of E_2 modes is lower and not sharper enough than that of ZnO. It implies decreasing lattice symmetry induced by indium substituting Zn site. Meanwhile, multiphonon processes of ZnO:In lattices are observed in the temperature-dependence PL spectra [Fig. 5(b)], which is excited by a He–Cd laser (325-nm line). This will be discussed later.

Figure 4 shows the PL spectrum of the ZnO and ZnO:In network excited by 325-nm UV light from He–Cd laser at room temperature. Optical-absorption spectra of the two samples on quartz substrates are shown in an inset. In Fig. 4, there are three interesting points worthy of discussion. First, the PL spectra of ZnO contain a strong UV band peak at 394 nm, and its full width at the half maximum (FWHM) is about 175 meV. Besides, a very weak broad green brand centered at about 550 nm occurred. The UV emission is originated from excitonic recombination corresponding to the near-band-edge emission of ZnO. The green emission peak is commonly referred to as a deep-level or trap-state emission. The green transition has been attributed to the singly ionized oxygen vacancy in ZnO and the emission results from the radiative recombination of a photogenerated hole with an electron occupying the oxygen vacancy.[17] The strong UV and weak green bands imply good crystal surface. Second, the UV emission peak position of ZnO:In thin films exhibits blueshift compared to that of ZnO. This is attributed to the shift of the optical band gap in these nanorods. According to the optical-absorption spectra, pronounced exciton absorption peaks are obvious near the absorption edge. Exciton absorption peak positions of ZnO and ZnO:In are 378 and 363 nm, respectively. So the band gap should be calculated in terms of the equation $E_g = P_1 + \Delta E_b$,[18] where P_1 and ΔE_b are the absorption peak position of exciton and the exciton binding energy of 60 meV, respectively. As a result, the optical band gaps of ZnO and ZnO:In obtained from the inset are 3.34 and 3.47 eV, respectively. The optical band gap of ZnO:In is larger than that of pure ZnO due to Burstein-Moss shift.[19] There are more electrons contributed by indium dopants that take up the energy levels located at the bottom of conduction band. When ZnO:In samples were excited with a He–Cd laser at 325 nm, excitons take up higher-energy levels at the bottom of conduction band than that of ZnO. Radiative recombination of these excitons will lead to a blueshift and broaden of UV emission peak. Finally, the intensity of UV emission peak decreases apparently after In doping, and its FWHM is about 179 meV. The PL integrated intensity ratio of the UV emission to the deep-level green emissions (I_U/I_D) is 7.5 and 1.2, for ZnO and ZnO:In samples, respectively. We ascribe the decrease of the UV emission intensity and I_U/I_D after indium doping to the weak exciton Coulomb interaction effect. In act as scattering centers of dopant and generate screened Coulomb potential field, which makes excitons ionized because of losing the Coulomb interaction effect. As a result, exciton effect decreases obviously, and the intensity of near-band-edge luminescence reduces. However, this phenomenon will be expected in the appearance of strong multiphonon resonant Raman scattering in ZnO:In rods. It will be observed in Fig. 5(b). In incorporation impedes the radiative recombination of excitions, on the contrary, it improves the possibility of the producing of photocurrent. This may be useful for photoelectric devices application.

Figure 5 shows the temperature-dependent PL spectra of undoped ZnO (a) and In-doped ZnO (b) samples at the temperature ranging from 79 to 299 K. The integrated intensity of the UV emission of both samples was illustrated in Fig. 5(c). It is noticed that the PL spectrum of undoped ZnO shows only one UV emission peak at near-band-edge of

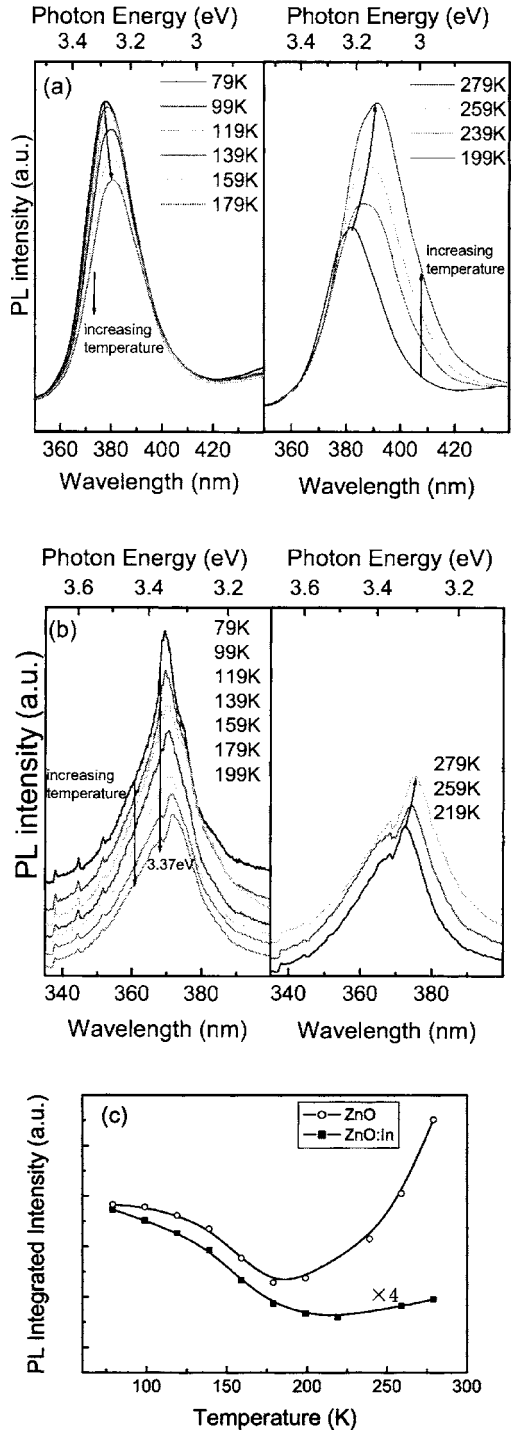

FIG. 5. Temperature-dependent PL spectra for (a) undoped ZnO and (b) In-doped ZnO on quartz substrates. (c) The temperature dependence of PL integrated intensity of ZnO and ZnO:In samples.

3.29 eV. This band is not sharp enough, and its FWHM is about 154 meV. This broadening of the PL band can be accounted for the high concentration of intrinsic defects. The broadened band involves excitons bound to neutral donors. In good-quality bulk samples, a number of sharp separate lines will be observed in this region and are assigned to neutral-bound-exciton complexes. In our cases, this line is inhomogeneously broadened due to an overlapping of several lines. In usual ZnO films or bulk crystals, free exciton emissions are rarely observed at low temperatures because of the localization of excitons by impurities, especially by donors. At higher temperatures (usually over 60 K), on the other hand, free exciton emissions appear because of the ionization of impurities that used to be bound excitons at low temperatures.[20] The absence of free exciton emissions in the PL spectra suggests that there is a certain concentration of the impurities in these rodlike structures. With increasing temperature, the peak position has a redshift, and PL intensity is slowly quenched due to the thermal ionization of exciton and thermally activated nonradiative recombination mechanisms, as shown in Fig. 5(c).

The UV emission band shows a strong emission with enhanced temperature above 217 K. This abnormal phenomenon can be attributed to the appearance of band-to-impurity transitions.[21–24] The impurity involved is the one having larger binding energy, because the one with smaller binding energy is ionized at elevated temperature. Due to the larger binding energy of the acceptor in ZnO, the band-to-impurity transition is attributed to conduction-band-to-acceptor transition in which free electrons in the conduction band recombine with acceptors.

For the PL emission spectra of In-doped ZnO samples [Figs. 5(b) and 5(c)], the integrated intensity and the shift of peak position of UV emission have a similar feature to that of ZnO. The interesting peak at 3.37 eV (368 nm) is identified by the local state emission because its peak position is not changed with the increase of the temperature in all temperature ranges.

The other interesting phenomenon is that the modes originating from the multiphonon-scattering process by second- (337.7 nm and 1157 cm^{-1}), third- (344.4 nm and 1733 cm^{-1}), fourth- (351.5 nm and 2319 cm^{-1}), and fifth-order (358.6 nm and 2883 cm^{-1}) LO phonons resonant lines are clearly observed in the spectra under resonant excitation by the 325-nm laser line, which was superimposed on a broad PL band. However, these LO phonon resonant lines cannot be found for ZnO samples. It is ascribed to the extrinsic dopant. Indium is incorporated into ZnO nanorods, substitutes for Zn site partly and acts as a donor to contribute free carrier. The appearance of more LO phonon resonant lines is accounted for these free carriers. This is in accordance with the weak near-band-edge emission of In-doped ZnO in PL spectra (Fig. 4). Impurities produce screened Coulomb potential field and reduce the UV luminescence intensity.

IV. CONCLUSIONS

In conclusion, we have fabricated ZnO and ZnO:In nanorod thin films on quartz substrates in aqueous solution by sol-gel method. The structure, morphology, and optical properties were characterized. All the samples have a typical hexagonal wurtzite structure. No single In_2O_3 phase in ZnO lattice is observed according to the XRD and Raman spectra. The samples possess high crystalline. The PL spectra of ZnO show a strong UV emission band located at 394 nm and a very weak visible emission associated with the singly

ionized oxygen vacancy. The shift of optical band gap, quenching of the near-band-edge photoluminescence, and enhancement of LO modes multiphonon resonant Raman scattering in ZnO:In crystals can be attributed to In incorporation. Abnormal temperature dependence of UV emission integrated intensity of ZnO and ZnO:In samples is observed. The local state emission peak at 3.37 eV in ZnO:In sample is observed in low temperature. The near-band-edge emission peak at room temperature is a mixture of excitons and impurity-related transitions for these samples.

ACKNOWLEDGMENTS

This work is supported by the National Natural Science Foundation of China Grant Nos. 60376009 and 60278031, the Major Project of the National Natural Science Foundation of China Grant No. 60336020, and the Cultivation Fund of the Key Scientific and Technical Innovation Project, Ministry of Education of China Grant No. 704017.

[1] V. Srikant and D. R. Clarke, J. Appl. Phys. **83**, 5447 (1998).
[2] N. Saito, H. Haneda, T. Sekiguchi, N. Ohashi, I. Sakaguchi, and K. Koumoto, Adv. Mater. (Weinheim, Ger.) **14**, 418 (2002).
[3] S. Liang, H. Sheng, Y. Liu, Z. Hio, Y. Lu, and H. Shen, J. Cryst. Growth **225**, 110 (2001).
[4] Y. Lin, Z. Zhang, Z. Tang, F. Yuan, and J. Li, Adv. Mater. Opt. Electron. **9**, 206 (1999).
[5] N. Golego, S. A. Studenikin, and M. Cocivera, J. Electrochem. Soc. **147**, 1592 (2000).
[6] T. Minami, H. Sonohara, T. Kakumu, and S. Takata, Jpn. J. Appl. Phys., Part 2 **34**, L971 (1995).
[7] J. M. Phillips, R. J. Cava, G. A. Thomas *et al.*, Appl. Phys. Lett. **67**, 2246 (1995).
[8] H. Takatsuji, T. Hiromori, K. Tsujimoto, S. Tsuji, K. Kuroda, and H. Saka, Mater. Res. Soc. Symp. Proc. **508**, 315 (1998).
[9] T. Minami, J. Vac. Sci. Technol. A **17**, 1765 (1999).
[10] Y. S. Jung, J. Y. Seo, D. W. Lee, and D. Y. Jeon, Thin Solid Films **445**, 63 (2003).
[11] J. Jie, G. Wang, X. Han, Q. Yu, Y. Liao, G. Li, and J. G. Hou, Chem. Phys. Lett. **387**, 466 (2004).
[12] S. Y. Bae, H. C. Choi, C. W. Na, and J. Park, Appl. Phys. Lett. **86**, 033102 (2005).
[13] J. G. Wen, J. Y. Lao, D. Z. Wang, T. M. Kyaw, Y. L. Foo, and Z. F. Ren, Chem. Phys. Lett. **372**, 717 (2003).
[14] L. Vayssieres, Adv. Mater. (Weinheim, Ger.) **15**, 464 (2003).
[15] R. Loudon, Adv. Phys. **13**, 423 (1964).
[16] C. A. Arguello, D. L. Rousseau, and S. P. S. Porto, Phys. Rev. **181**, 1351 (1969).
[17] K. Vanheusden, W. L. Warren, C. H. Seager, D. K. Tallant, J. A. Voigt, and B. E. Gnade, J. Appl. Phys. **79**, 7983 (1996).
[18] Y. P. Varshni, Physica (Amsterdam) **34**, 149 (1967).
[19] E. Burstein, Phys. Rev. **93**, 632 (1954).
[20] A. Zeuner, D. M. Hofmann, B. K. Meyer, M. Heuken, J. Bälsing, and A. Krost, Appl. Phys. Lett. **80**, 2078 (2002).
[21] K. Thonke, Th. Gruber, N. Teofilov, R. Schönfelder, A. Waag, and R. Sauer, Physica B **308–310**, 945 (2001).
[22] D. J. As, F. Schmilgus, C. Wang, B. Schöttker, D. Schikora, and K. Lischka, Appl. Phys. Lett. **70**, 1311 (1997).
[23] J. F. Wang, D. Masugata, C. B. Oh, A. Omino, S. Seto, and M. Isshiki, Phys. Status Solidi A **193**, 251 (2002).
[24] B. P. Zhang, N. T. Binh, Y. Segawa, K. Wakatsuki, and N. Usami, Appl. Phys. Lett. **83**, 1635 (2003).